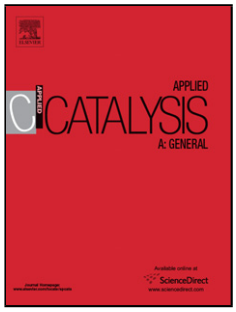

High Performance of Supported Cu-based Catalysts Modulated via Phosphamide Coordination in Acetylene Hydrochlorination

Yubing Hu (Investigation) (Writing - original draft), Yan Wang, Yulian Wang, Wei Li (Resources), Jinli Zhang (Resources), You Han (Supervision)<ce:contributor-role>Writing- Review and editing) (Project administration) (Funding acquisition)

PII: S0926-860X(20)30001-6

DOI: https://doi.org/10.1016/j.apcata.2020.117408

Reference: APCATA 117408

To appear in: *Applied Catalysis A, General*

Received Date: 10 October 2019

Revised Date: 30 December 2019

Accepted Date: 1 January 2020

Please cite this article as: Hu Y, Wang Y, Wang Y, Li W, Zhang J, Han Y, High Performance of Supported Cu-based Catalysts Modulated via Phosphamide Coordination in Acetylene Hydrochlorination, *Applied Catalysis A, General* (2020), doi: https://doi.org/10.1016/j.apcata.2020.117408

High Performance of Supported Cu-based Catalysts Modulated via Phosphamide Coordination in Acetylene Hydrochlorination

Yubing Hu [a], Yan Wang [a], Yulian Wang [a], Wei Li [a], Jinli Zhang [a,b] and You Han [a,*]

[a] School of Chemical Engineering and Technology, Tianjin University, Tianjin 300072, China

[b] School of Chemistry and Chemical Engineering, Shihezi University, Shihezi 832003, China

Author information

Corresponding Author

You Han (E-mail: yhan@tju.edu.cn)

Notes

The authors declare no competing financial interest

Graphical Abstract

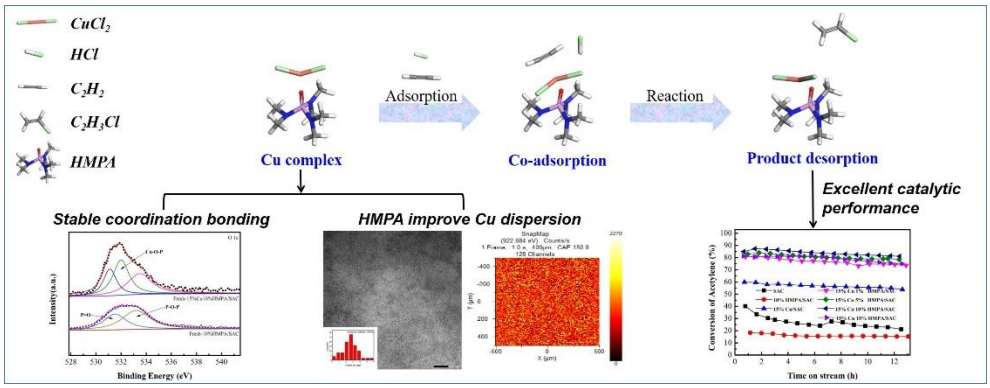

Highlights

- A series of supported Cu complex catalysts were prepared with phosphoramide ligands and had high efficiency in the acetylene hydrochloride reaction.
- The catalyst with optimal HMPA ligand exhibited good stability in the 100 h lifetime test.
- HMPA ligand can restrain the coke deposition, suppress the loss of loading Cu, and stabilize the valence state of active Cu species.
- Due to the electron transfer mechanism, a stable coordination structure formed between the Cu and HMPA via Cu-O binding.

Abstract

In order to develop a cut-price, high-efficiency non-mercuric catalyst for acetylene hydrochlorination reaction, several kinds of supported Cu-based catalysts containing phosphoramide ligands have been synthesized by wet impregnation

method. The outstanding catalytic activity was obtained over 15%Cu10%HMPA/SAC catalyst with acetylene conversion of 87.25% in the test conditions of T = 180 °C, $GHSV(C_2H_2)$ = 180 h^{-1} and V(HCl): $V(C_2H_2)$ = 1.2. The catalyst with optimal HMPA ligand also exhibited splendid stability in 100 h lifetime test. The analysis for XRD, TEM, TGA, ICP, H_2-TPR and XPS indicated that HMPA ligand can improve Cu species dispersion, restrain coke deposition, suppress loss of loading Cu, and stabilize valence state of active Cu species. Due to electron transfer mechanism, steady coordination structure between Cu and HMPA led to favorable properties of Cu-based catalyst, which was further proved by FT-IR, Raman spectra, O 1s XPS spectra integrated with DFT calculations.

Keywords: Phosphoramide ligand, Cu-based catalyst, Coordination, Acetylene hydrochlorination

1. Introduction

Ligands are widely used in the field of catalysis because they can form a stable coordination structure with metals and thus stabilizing the metal valence state in the catalysts, thereby preventing the catalyst deactivation caused by metal nanoparticles agglomeration, which is the main reason for the loss of active sites, in reverse obtaining high surface areas to provide more active metal area [1]. Therefore, the role of ligands in the territory of nanoparticle catalysis has been paid more and more attention [2-4] and has been reported to influence a great many of factors of the catalysts, including the properties of electron [5], the oxidation state of the metal [6], the spatial environment of the active sites [7-8], the variation of hydrophobicity [9]

and the blocking of toxic sites [10].

Copper is more ubiquitous and more affordable compared with the noble metals, hence a great many of trials devoted on the utilization of copper in catalysis have been explored in the light of the economical efficiency and sustainability [11-12]. Due to the multifunctionality of design, Cu-based complexes can effectively adjust the reaction rate, conversation, selectivity, yield, and even can change the catalytic mechanism during the reaction processes [13-14]. Combined with the advantages of ligand and copper, the Cu-based complexes can be served as catalyst for a comprehensive range of reactions [15-16], for instance, cross-coupling of the C-C [17] and C-Heteroatom [18], oxidation of alkanes [19], C-H functionalization [20], synthesis of heterocyclic [21], asymmetric conjugate additions [22] and click chemistry [23]. However, the application of Cu complexes in the hydrochlorination of acetylene is very limited [24].

Acetylene hydrochlorination reaction is a crucial industrial process for fabricating the third largest plastic-vinyl chloride (VCM) in the world. VCM is the monomer that produces the third most generally utilized plastic polyvinyl chloride (PVC) in our lives. The traditional supported catalyst for the hydrochlorination of acetylene is $HgCl_2$/AC, which is virulent, evaporable and pernicious to human health and environment [25-26]. Cu as an alternative for noble metals holds a significantly place for further investigating an efficient and eco-friendly catalyst in the industry process of PVC manufacturing. Although the Cu-based catalyst with certain catalytic properties for hydrochlorination of acetylene is obtained, the largest problem of the

Cu catalyst is the deactivation which is mainly arised from metal active sites aggregation and reduction of high valence state of copper. This is a tremendous challenge to improve the stability of the Cu-based catalyst thereby enhancing the catalytic performance [27]. In order to settle the conundrum of catalyst deactivation, a series of efforts in the modification on Cu-based catalyst for acetylene hydrochlorination have been performed. For instance, Li et al reported the appropriate phosphorus doping promotes copper species dispersion, increases the reciprocity between the Cu catalyst and the support, and suppresses the copper species aggregation during the acetylene hydrochlorination process [28]. Zhai et al prepared carbon-supported perovskite-like $CsCuCl_3$ double nonprecious metal catalyst for acetylene hydrochlorination to improve the HCl adsorption and maintain Cu^{2+} species [29]. Zhou et al introduced the N-CNTs as a support to increase acetylene adsorption capacity thus significantly improving catalytic performance [30]. Wang et al imported MOMTPPC ionic liquid to Cu-based catalyst, thus realizing the obvious catalytic activity enhancement [31]. It is worth mentioning that the modification methods for Cu-based catalysts in the above studies are mainly the addition of auxiliaries or the second metal and decoration of support, scarcely any synthesis of Cu complex through the formation of stable coordination bond between Cu and ligand. Recently, Wang et al prepared the HEDP ligand modified Cu-based catalyst with relatively 83.4% acetylene conversion and catalytic stability of only 20 h. The catalytic activity of Cu-1HEDP/AC catalyst is inferior to that of the noble catalyst and industrial catalyst due to the structure of the ligand [24].

In this work, we select four types of phosphoramide ligand containing N and P to form Cu complexes because phosphoramide ligand has a range of good properties including PVC weatherability, favorable solubility and low cost, especially the possible synergistic effect of phosphorus and nitrogen, the molecular structure of the phosphoramide ligands are shown in Figure S1. Four kinds of carbon-supported Cu complex catalysts containing these phosphoramide ligands were synthesized using a portable method of the wet impregnation to explore the effect of ligand contents and functional groups for disparate phosphoramide materials on catalytic performance. Furthermore, the scientific characterizations combined DFT simulations were analyzed to reveal the coordination structure between the Cu and HMPA ligand. The HMPA modified Cu catalyst possesses further industrial application potential in acetylene hydrochlorination. The cheap, environmentally-friendly and easy prepared Cu-based catalyst will facilitate the continuable PVC industry progress.

2. Experimental and theoretical method

2.1 Materials.

The following experimental materials were used in the research: copper chloride ($CuCl_2$, purity 98%) was purchased from Shanghai Aladdin Bio-Chem Technology Co., Ltd. Hexamethylphosphoramide (HMPA) was purchased from Shanghai D&B Biological Science and Technology Co. Ltd., with the purity higher than 99%. Tris (N,N-tetramethylene) phosphoric acid triamide (TPPO) was purchased from Shanghai Titanchem Co., Ltd., with the purity higher than 98%. Diethyl PhosphoraMidate (NSC, purity 98%) was purchased from TCI (Shanghai) Development Co., Ltd.

Cyclophosphamide hydrate (CTX) was purchased from Shanghai D&B Biological Science and Technology Co. Ltd., with the purity higher than 97%. Spherical activated carbon (marked as SAC, 20-40 mesh) was purchased from Shandong Jining Chengguang Coal Chemical Co., Ltd. Hydrogen chloride (HCl, purity >99.99%) was purchased from Tianjin Dongxiang special gas Co., Ltd and acetylene (C_2H_2, purity >99.99%) was purchased from Tianjin Huanyu Gas Co., Ltd. All experimental materials were not further purified prior to use.

2.2 Catalyst preparation.

The SAC support Cu-based catalysts were synthesized through wet impregnation method with the solvent of deionized water. We take the preparation process of 15%Cu1%HMPA/SAC for an example. First, 1.6192 g $CuCl_2$ and 0.05 g HMPA were dissolved in 10 mL deionized water and stirred intensely until a blue, transparent solution formed. Then 5 g SAC was slowly poured into the liquor above with stirring under room temperature. Subsequently, the obtained mixture was treated with ultrasonic for 15 min and was incubated at 60 ^oC for 12 h. Finally, the fresh catalyst was acquired after desiccating at 120 ^oC for 12 h, denoted as 15%Cu1%HMPA/SAC. Furthermore, catalysts with different mass fraction of HMPA including 5%, 10%, 15%, named as 15%Cu5%HMPA/SAC, 15%Cu10%HMPA/SAC, 15%Cu15%HMPA/SAC, respectively, were prepared to optimize the content of HMPA for improving the catalytic performance. As a control, the 15%Cu/SAC and the 10%HMPA/SAC were synthesized with the same method only without HMPA ($CuCl_2$).

In addition, other three catalysts containing disparate phosphoramide ligands were prepared using the same method above instead of the solvent to ethanol, including 15%Cu10%TPPO/SAC, 15%Cu10%NSC/SAC and 15%Cu10%CTX/SAC. The Cu content in all Cu-based catalysts was 15 wt %.

2.3 Catalyst characterization.

X-ray diffraction (XRD) of the catalysts was performed to determine dispersity and crystallinity of the active component and cystal form of the support by the SmartLab X-ray diffracometer with Cu Kα radiation (9 KW) over the range $10° \leq 2\theta \leq 80°$ at a scan rate of 10^{o} min^{-1}.

Transmission electron microscopy (TEM) and scanning transmission electron microscopy (STEM) were conducted to detect morphologies of catalysts and to observe the distribution and the size of Cu particles using JEM 2100F (JEOL, Japan) with the acceleration voltage of 200 kV.

X-ray photoelectron spectra (XPS) was measured by K-Alpha+ (Thermo Fisher, USA) to distinguish chemical elements valence states of the catalyst surface. The standard C 1s spectra of carbon (284.8 eV) was employed to adjust the binding energies.

Low-temperature N_2 adsorption/desorption experiments were carried out on the Quantachrome Autosorb Automated Gas Sorption System to test the various texture parameters of the catalysts. The catalysts were heated at 200 °C and outgassed for 4 h and measured using liquid nitrogen adsorption at -196 °C. The BET method and the density functional theory (DFT) method were used to calculate the surface areas and

the pore size distribution of the catalysts, respectively.

Hydrogen temperature-programmed reduction (H_2-TPR) of the catalysts was detected to investigate the reduced ability of the catalysts using Quantachrome Instruments AMI-90. The H_2-TPR was operated from 50 to 1000 ^oC in 130 mL min^{-1} gas flow (10 vol% H_2/Ar) at a ramp rate of 10 °C min^{-1}. H_2 consumption was determined by TCD detector.

Thermogravimetric analysis (TGA) was performed on METTLER TOLEDO TGA/DSC 2 instrument to research the thermostability and coke depositions of the catalysts. The test temperature was increased from 30 to 800 °C at a 10 °C min^{-1} heating rate under a 50 mL min^{-1}air flow.

Inductively coupled plasma-optical emission spectrometry (ICP-OES) was measured to determine the loading of Cu for the catalysts with 725-ES instrument (Varian, USA).

Fourier transform infrared spectra (FT-IR) was carried out by Bruker Vertex70 FT-IR spectrophotometer containing a DTGS detector. The experiments were conducted from 500 to 4000 cm^{-1} with 32 scanning times under the 4 cm^{-1} resolution.

The Raman spectra of the catalysts was measured by the HR Revolution (HORIBA, France) using a argon ion laser (532 nm) to excite within the scope of 200 to 2300 cm^{-1}.

2.4 Catalyst tests.

The catalytic performance of multiple catalysts was tested in the continuous fixed bed tubular reactor (i.d. 10 mm) for acetylene hydrochlorination under the

atmospheric pressure. 3 mL prepared catalyst was introduced to the fixed position of the tubular reactor. After that, nitrogen gas at a suitable flow was imported to the system to purge the air and vapor sustaining before reaction. Subsequently, N_2 was closed and purified hydrogen chloride (HCl) (10.8 mL min^{-1}) was introduced to the tube reactor to activate catalyst at 180 ^oC for 30 min. Finally, clean acetylene (C_2H_2) was passed through the reactor at 9 mL min^{-1}. The C_2H_2: HCl ratio was 1:1.2, the gas hourly space velocity (*GHSV*) of acetylene was 180 h^{-1}. In addition, excess HCl in the gaseous product were absorbed by absorption bottles containing solution of sodium hydroxide (NaOH). Finally, the outcome analysis was carried out using GC-2014C gas chromatograph equipped with a flame ionization detector (FID).

2.5 Simulation details.

We selected $DMol^3$ module of Materials Studio software (Accelrys Inc) to operate all of the relevant density functional theory (DFT) calculations. In order to handle the correlation and exchange, Perdew-Wang-91 (PW91) within the formulation of the generalized gradient approximation (GGA) was adopted in geometry optimizations. The DNP basis set and the all-electron-core were applied in the whole calculations. The criterion of the energy convergence was fixed at 0.00001 Ha, the atomic structures were relaxed until all unconstrained atoms forces were < 0.002 Hartree $Å^{-1}$. The smearing for the orbital occupation was set as 0.005 Ha to realize convergence of the self-consistent field. To better understand electron transfer mechanism between $CuCl_2$ and HMPA ligand, the Mulliken analysis is also carried out.

3. Results and discussion

3.1 Catalytic performance of Cu-based catalysts.

As the representative phosphoramide ligand, the influence of different mass fraction of HMPA on catalytic activity was studied firstly, and the results are shown in Figure 1. The 15%Cu/SAC owns an incipient acetylene conversion of 59.80%, while the acetylene conversion on pure 10%HMPA/SAC is only 17.30%. However, the acetylene conversion on the 15%Cu1%HMPA/SAC rises to 81.12% when only 1% HMPA is added to the catalyst. Compared to the pure 15%Cu/SAC catalyst, the acetylene conversion on the 15%Cu1%HMPA/SAC significantly increases by 21.32%. The acetylene conversion on the catalysts of 15%Cu5%HMPA/SAC and 15%Cu10%HMPA/SAC continues to rise obviously to 83.97% and 87.25%, respectively, with the increase of HMPA content. The Cu-based catalyst with 10 wt % HMPA content possesses the maximum of acetylene conversion (87.25%), which is higher than the Cu-based catalyst conversion reported in the vast majority of literatures for acetylene hydrochlorination under approximate reaction conditions, as listed in Table S1. It is worth noting that the acetylene conversion on the 15%Cu10%HMPA/SAC (87.25%) is even much higher than the sum of acetylene conversion on pure 15%Cu/SAC and pure 10%HMPA/SAC (77.10%). As a consequence, we infer that synergy between the copper species and the HMPA may be a reason for the highest conversion of acetylene over the 15%Cu10%HMPA/SAC catalyst. when the HMPA content reaches 15 wt %, the acetylene conversion does not increase but decreases to 81.37%. Meanwhile, the selectivity of the VCM for the

catalysts mentioned above attains nearly overtops 99% except that of pure 10%HMPA/SAC catalyst, as shown in Figure 1b.

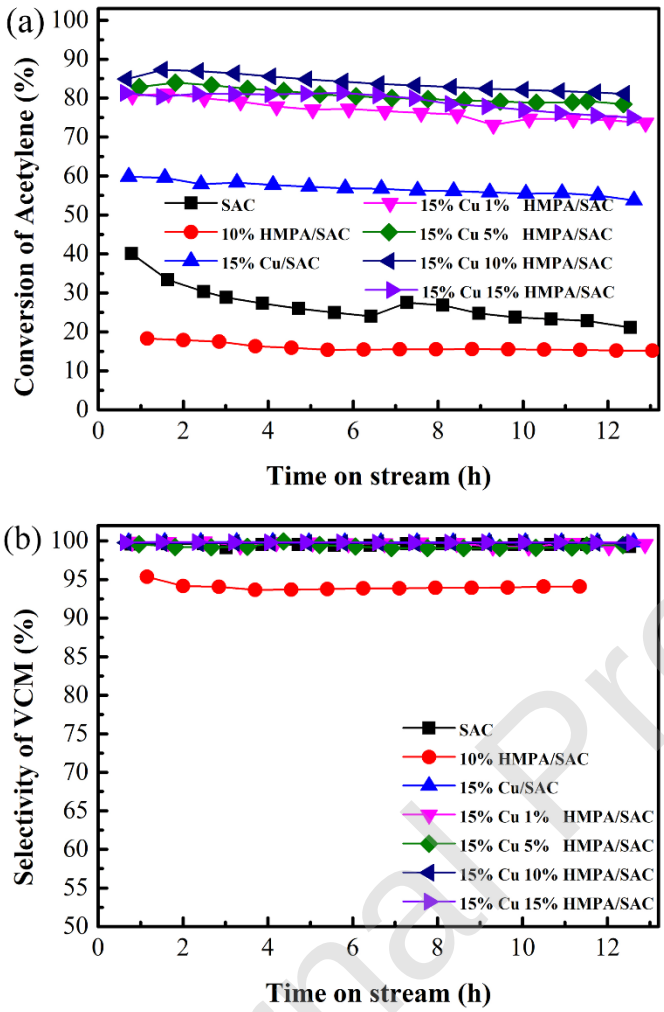

Figure 1. Acetylene conversion (a) and VCM selectivity (b) of Cu-based catalysts with different HMPA content for acetylene hydrochlorination. Test conditions: T = 180 °C, $GHSV(C_2H_2)$ = 180 h^{-1}, $V(HCl)$: $V(C_2H_2)$ = 1.2.

Furthermore, catalytic properties of the catalysts containing other three disparate phosphoramide ligands including TPPO, NSC and CTX, respectively, are also investigated at the same test conditions. As shown in Figure 2, the conversion of

acetylene on the 15%Cu10%TPPO/SAC, 15%Cu10%NSC/SAC and 15%Cu10%CTX/SAC achieves to 78.68%, 83.95% and 80.86%, respectively, which all far exceed the acetylene conversion of the pure 15%Cu/SAC but slightly lower than that of 15%Cu10%HMPA catalyst with the same ligand mass fraction. At the same time, Figure 2b shows the VCM selectivity on the three catalysts containing different phosphoramide ligands is all above 93%. In summary, the phosphoramide ligands can truly improve the catalytic performance because of reciprocity between the phosphoramide ligands and the copper.

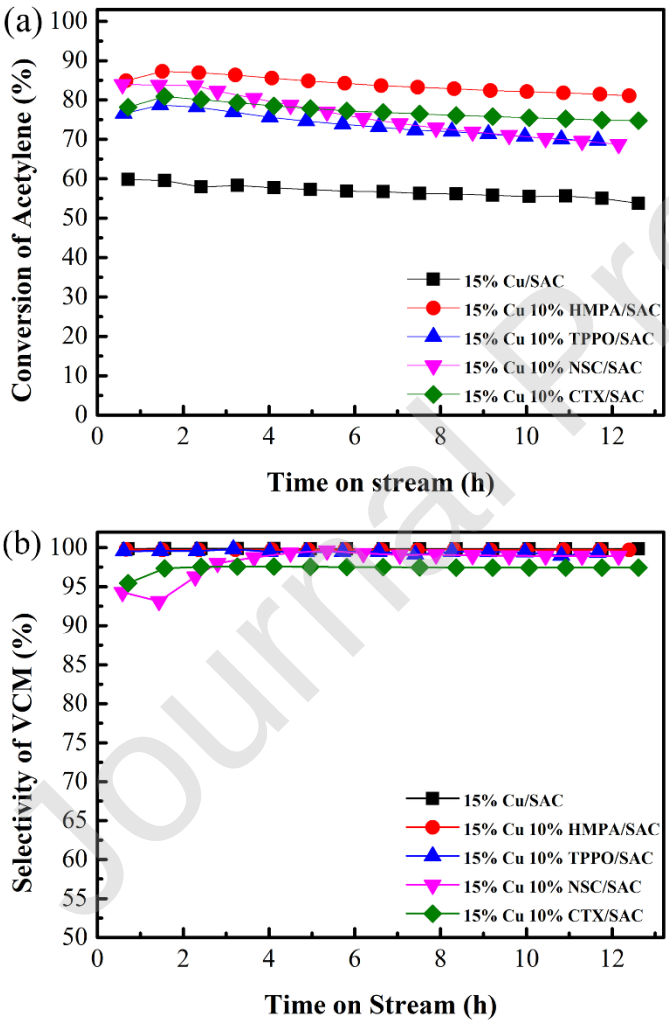

Figure 2. Acetylene conversion (a) and VCM selectivity (b) of Cu-based catalysts containing

different phosphoramide ligands for acetylene hydrochlorination. Test conditions: T = 180 °C, $GHSV(C_2H_2)$ = 180 h^{-1}, and V(HCl): $V(C_2H_2)$ = 1.2.

With the purpose of industrial application, long-term stability experiments of the 15%Cu10%HMPA/SAC with the optimal HMPA loading are tested under different *GHSVs*. Primarily, the catalytic performance of 15%Cu10%HMPA/SAC catalyst at the industrial *GHSV* of 50 h^{-1} is investigated. As shown in Figure 3a, the initial acetylene conversion just reaches 94.38% and rises to the maximum of 97.07% gradually after about 20 h. Subsequently, the conversion of acetylene decreases slightly to 90.03% within 100 h reaction time, indicating that the HMPA ligand promotes the stability of Cu-based catalyst significantly, compared to the reported durability data of Cu-based catalysts utilized in acetylene hydrochlorination. The 15%Cu10%HMPA/SAC catalyst stability is further inspected under the harsh condition of *GHSV* = 90 h^{-1}. The acetylene conversion of 15%Cu10%HMPA/SAC achieves 96.68% and then reduces to 86.49% after testing time of 100 h, illustrating that the conversion of acetylene only declines 3.15% more than that for the same catalyst at *GHSV* = 50 h^{-1} at the same time. The results further confirm that the Cu-based catalyst with HMPA ligand possesses excellent durability even though in the harsher conditions. Moreover, the VCM selectivity for the catalyst maintains above 99% during the lifetime testing.

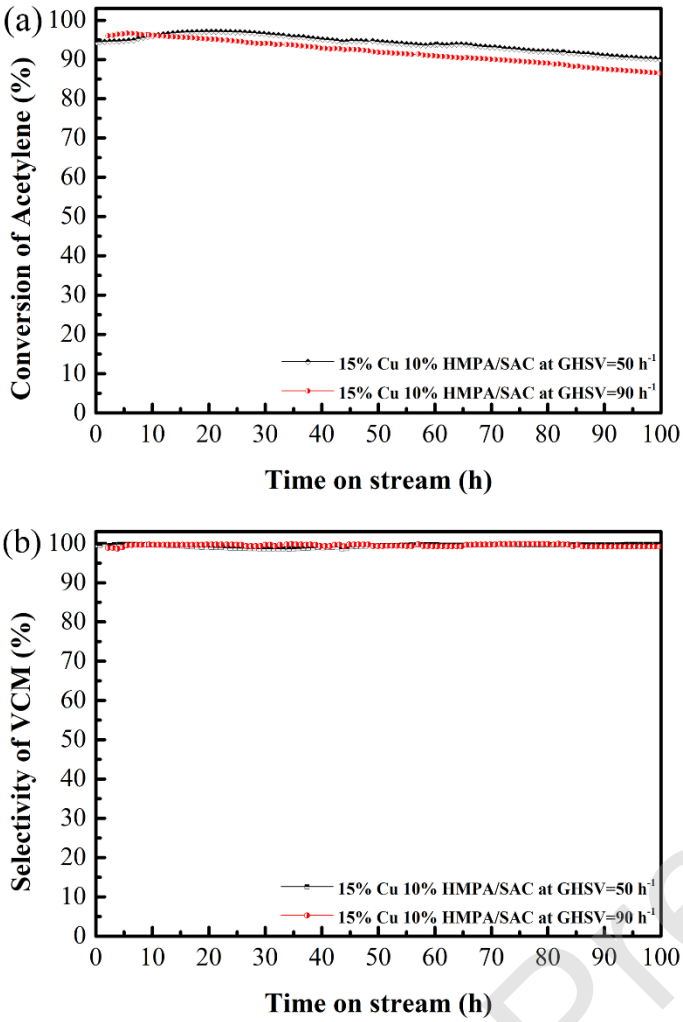

Figure 3. Acetylene conversion (a) and VCM selectivity (b) of 15%Cu10%HMPA/SAC catalyst for acetylene hydrochlorination. Test conditions: T = 180 °C, $GHSV(C_2H_2)$ = 90 h^{-1} (50 h^{-1}), and V(HCl): $V(C_2H_2)$ = 1.2.

3.2 HMPA improves Cu species dispersity.

Figure 4 displays the XRD patterns for disparate catalysts. Two dominating diffraction peaks at around 25° and 43° can be ascribed to the (002) and (101) planes of the SAC support, respectively [28, 32]. It is worth noting that three extra low intensity diffraction peaks of about 16°, 32° and 40° can be assigned to the copper atacamite ($Cu_2Cl(OH)_3$) based on the JCPDS file data of Fresh-15%Cu/SAC catalyst

compared with pure SAC [28]. We infer that the reason for other three small diffraction peaks detected is the low dispersity of the copper active sites in catalyst, which is caused by the aggregation of copper atacamite substance ($Cu_2Cl(OH)_3$). Compared with Fresh-15%Cu/SAC, $Cu_2Cl(OH)_3$ diffraction peaks at 32° and 40° of the Fresh-15%Cu1%HMPA/SAC disappear obviously and the peak at 16° becomes weak and broad, which indicates a handful of HMPA indeed improve the dispersity of the Cu species effectively. Subsequently, the diffraction peak of 16° belonging to $Cu_2Cl(OH)_3$ on 15%Cu5%HMPA/SAC vanishes completely. When the HMPA content is 10 wt %, no other discernible reflection except the two diffraction peaks of amorphous carbon can be detected and the curve becomes smooth greatly, indicating that the HMPA containing N and P can suppress copper species crystallization and enhance the Cu active sites dispersity significantly. Furthermore, the intensity and the area of the three diffraction peaks at about 16°, 32° and 40° for the Used-15%Cu/SAC increase slightly compared to those of pure Fresh-15%Cu/SAC, indicating that the level of the Cu species aggregation becomes serious. In contrast, the three diffraction peaks did not appear in both the fresh and used 15%Cu10%HMPA catalyst, indicating that Cu active species spread around very well in fresh and used 15%Cu10%HMPA catalyst. The results demonstrate that HMPA ligand can inhibit Cu species agglomeration, thus promoting catalytic performance of Cu complex catalyst.

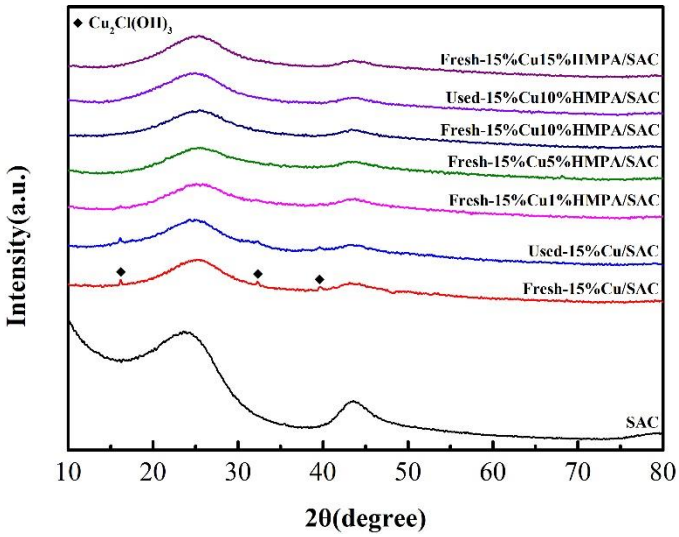

Figure 4. XRD patterns of the fresh and used Cu-based catalysts with different HMPA content.

In order to continue to analyze metal active sites dispersity, TEM photographs of pure Cu supported catalyst and 15%Cu10%HMPA/SAC before and after test are displayed in Figure 5. The mean metal grain size of Used-15%Cu/SAC catalyst is around 15.82 nm, which is far beyond that for Fresh-15%Cu/SAC catalyst (7.02 nm), demonstrating there is obvious Cu species aggregation in the reaction. Compared to pure 15%Cu/SAC after reaction, the mean grain size for Used-15%Cu10%HMPA/SAC catalyst is about 4.75 nm, which decreases significantly and is even lower than the mean particles diameter of the Fresh-15%Cu/SAC, illustrating that HMPA ligand can inhibit effectively Cu active sites agglomeration. It is worth mentioning that Fresh-15%Cu10%HMPA/SAC owns the minuscule average particles size of 2.59 nm, calculated on the basis of the 100 particles, which demonstrates that HMPA can promote availably Cu active sites dispersity thus gaining outstanding catalytic performance. For the Fresh-15%Cu10%HMPA/SAC catalyst, the elemental mapping using STEM mode is detected and shown in Figure 6. The elements mapping

of Cu, Cl, P, O and N proved that the main elements in the catalyst distribute symmetrically on the support surface, which intuitively certifies that the HMPA ligand enhances the dispersibility of Cu species due to the restraining of the growth of Cu particles size.

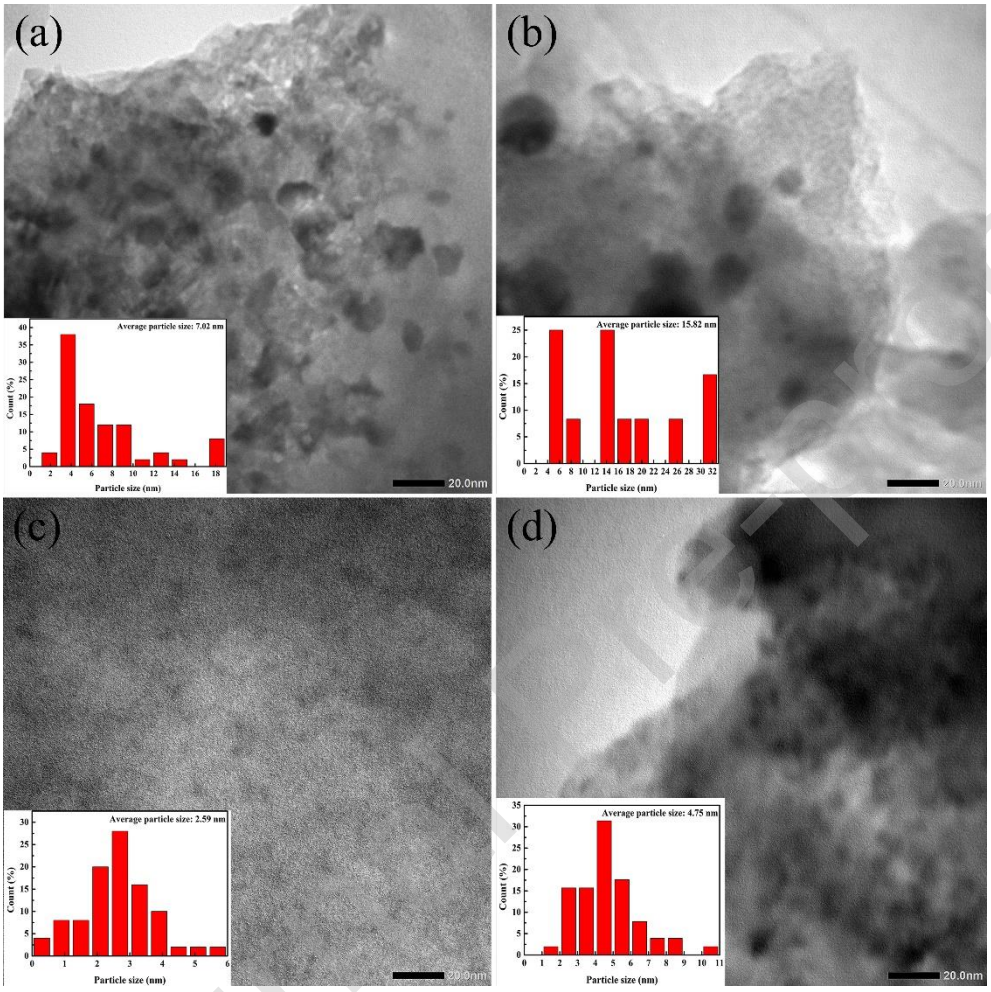

Figure 5. HRTEM images of fresh (a) and used (b) 15%Cu/SAC; fresh (c) and used (d) 15%Cu10%HMPA/SAC.

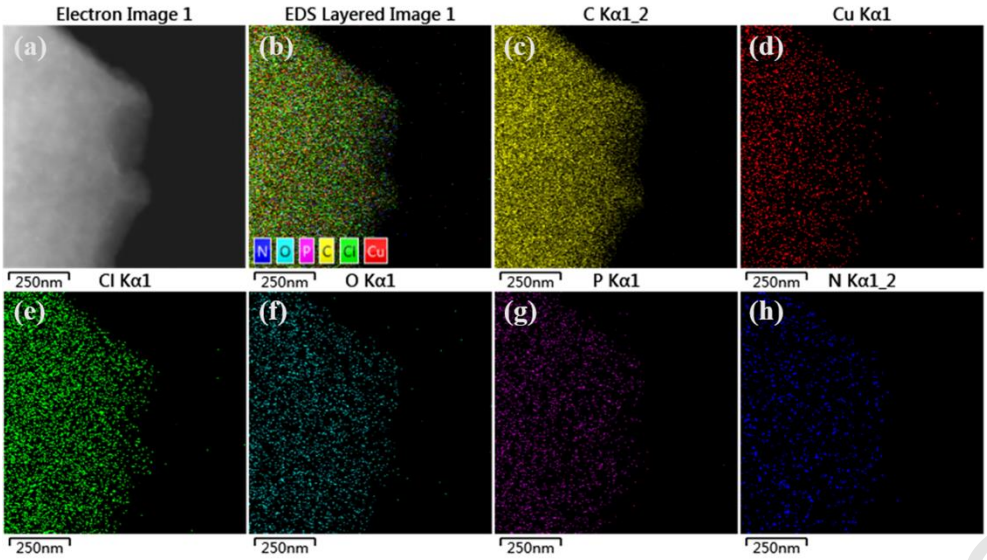

Figure 6. STEM photograph (a), elemental mapping image (b) for overlapping elements, elemental mapping images (c−h) of C, Cu, Cl, O, P, N, respectively.

Moreover, Figure 7 displays the XPS SnapMap of the fresh and used catalysts, which is a novel method to observe the dispersion of the Cu species. For instance, the yellow light and the red dark spots represent the high dispersity of Cu species and Cu cluster aggregation, respectively. Compared to the catalyst of Fresh-15%Cu/SAC (Figure 7a), the amount of yellow light spot corresponding to the high dispersed Cu species of the Fresh-15%Cu10%HMPA/SAC catalyst (Figure 7c) increases distinctly, indicating that the degree of aggregation Cu active sites decreases evidently via adding HMPA ligand. In addition, a large quantity of homogeneous light spots is also detected in Figure 7d, further demonstrating that proper HMPA content can promote Cu active sites dispersity thus one reason for excellent catalytic activity obtained on the 15%Cu10%HMPA/SAC catalyst.

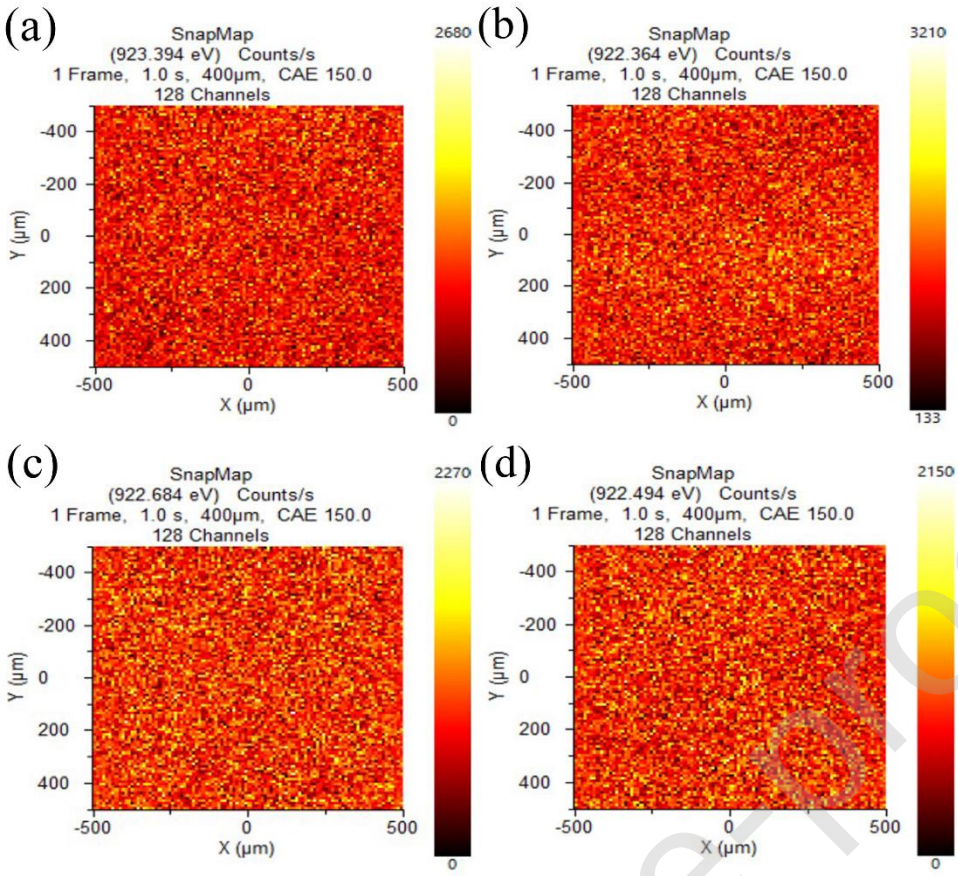

Figure 7. XPS SnapMap of fresh (a) and used (b) 15%Cu/SAC; fresh (c) and used (d) 15%Cu10%HMPA/SAC.

3.3 HMPA suppresses coke deposition and decreases Cu loss.

Thermo Gravimetric (TG) is detected to assess the amount of coke deposition and thermal stability of the catalysts, which is the main influence factors of the catalysts' deactivation [33]. Figure 8a and Figure 8b display the TGA experiments results of the 15%Cu/SAC and 15%Cu10%HMPA catalyst, respectively. The tiny weight loss before 100 ^{o}C can be recognized as the steaming of the water adsorbed on the catalysts. Notably, the distinct mass loss at the temperature range from 100 ^{o}C to about 300 ^{o}C is assigned to the used catalysts' surface carbon deposition [34]. The obvious quality loss above 300 ^{o}C may be attributed to the burning of SAC support

and HMPA ligand. When many researchers investigated the coke formation during the methane reforming reaction used Ni-based catalyst [35-38], they reported that the distinct main peak at high temperature above 300 °C possibly assigned to the coke form of carbon fibers. Therefore, there may be some inaccuracies in the calculation of coke deposition. In addition, pure 10%HMPA/SAC owns a higher decomposition temperature at approximately 600 ^{o}C as shown in Figure S2a, indicating the intense interaction between HMPA and the carbon support due to the favorable thermal stability of HMPA. Combining the TGA results of the Cu-based catalysts with other HMPA mass fraction as shown in Figure S2b-d, we can see that the more HMPA added to catalysts, the higher beginning temperature of the rapid weight loss. The results illustrate that HMPA possesses strong interaction with Cu and SAC, which can effectively improve the thermal stability.

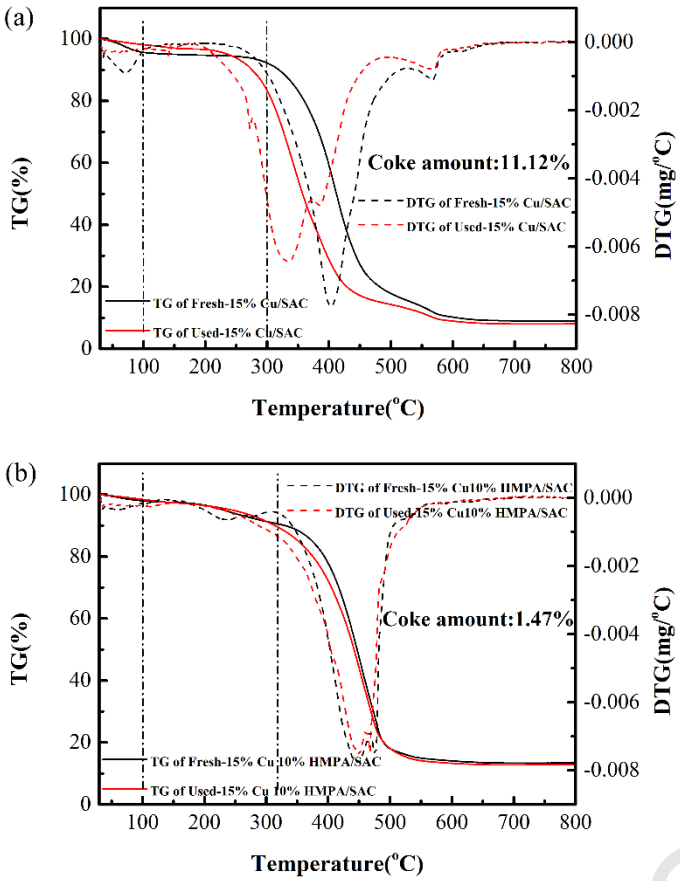

Figure 8. TGA and DTG splines of (a) 15%Cu/SAC and (b) 15%Cu10%HMPA/SAC before and after test.

The amount of carbon deposition of catalysts calculated using the contrastive method is listed in Table 1 [39-40]. It is worth noting that the 15%Cu/SAC exhibits the maximum of coke amount 11.12% and the lowest amount coke deposition of 1.47% is obtained on 15%Cu10%HMPA/SAC, declaring that the appropriate HMPA content of catalysts can restrain carbon deposition over surface of catalyst to the greatest extent.

Table 1. Content of Coke Deposition on Cu-based Catalysts

Catalysts	Content of coke deposition (%)
15%Cu/SAC	11.12
15%Cu1%HMPA/SAC	9.30
15%Cu5%HMPA/SAC	4.57
15%Cu10%HMPA/SAC	1.47
15%Cu15%HMPA/SAC	1.85

Furthermore, carbon deposition can lead to changes in pore structure parameters of catalysts. In order to further verify the accuracy of carbon deposition data, the Low-temperature nitrogen adsorption-desorption experiments are performed to research the influence of HMPA coordination on pore structure and specific surface area of catalysts before and after reaction, the results are shown in Table 2. Compared with pure Cu supported catalyst, the specific surface area and pore volume of the optimal catalyst with 10% HMPA content decrease slightly, which is mainly caused by dilution effect with the addition of HMPA ligand [28]. It is well known that carbon deposition reduces the specific surface area and pore volume of the catalyst. Notably, both $^{\triangle}S_{BET}$ and $^{\triangle}V_{total}$ of the optimal catalyst are smaller than those of the pure copper supported catalyst, which indicates that HMPA can effectively inhibit the coke deposition on the surface of the catalyst. The above analysis further corroborates the results of the TG tests.

Table 2. Pore Structure parameters of Cu-based catalysts before and after test.

Catalysts	S_{BET} (m^2 g^{-1})			V_{total} (cm^3 g^{-1})		
	Fresh	Used	$\triangle S_{BET}$	Fresh	Used	$\triangle V_{total}$
15%Cu/SAC	767	471	296	0.36	0.21	0.15
15%Cu10%HMPA/SAC	724	702	22	0.33	0.32	0.01

Since the catalyst deactivation is arised from the loss of Cu species active sites, Cu practical loading of the fresh and used catalysts is detected using ICP-OES, as listed in Table S2. The actual Cu loading amounts of the fresh pure Cu supported catalyst and the optimal HMPA modified catalysts are very close to 15 wt %. After reaction, the loss rate of copper content for pure Cu supported catalyst and the optimal HMPA modified catalysts are 5.24% and 4.61%, respectively. The result indicates that the addition of HMPA partly reduced the Cu loss during the reaction.

3.4 HMPA stabilizes the valence state of Cu species.

The H_2-TPR profiles of pure Cu supported catalyst and 15%Cu10%HMPA/SAC catalyst are performed to investigate the reducibility of the catalyst and the reciprocity among copper species, HMPA and the support. As shown in Figure 9, two main reduction peaks of fresh pure Cu supported catalyst at appropriately 451 ^oC and 516 ^oC can be detected, which are assigned to the reduction of Cu^{2+} species to Cu^+ particles and the change of Cu^+ to metallic copper, respectively. Different from traditional reduction range from 270 ^oC to 330 ^oC for Cu^{2+} to Cu^0, the reduction peaks of Cu^{2+} and Cu^+ shift to the higher temperatures, indicating that abundant Cu^{2+} in catalyst enhance the reduction difficulty thus obtaining the stronger reciprocity of Cu complex and SAC support [41]. The Cu^{2+} reduction peak of the Fresh-

15%Cu10%HMPA catalyst migrates to the higher temperature of 672 °C. Meanwhile, the peak corresponding to the Cu^{+} to Cu^{0} shifts to the higher temperature about 876 °C. The results illustrate that the reduction of high valence Cu is suppressed effectively because of the very strong reciprocity among the metal Cu, SAC support and HMPA. The fact that the H_2 consumption depended on the H_2 reduction peaks for the Fresh-15%Cu10%HMPA catalyst is much larger than that of the Fresh-15%Cu/SAC indicates that the reduction of Cu complex catalyst consumes more H_2, which confirms that the HMPA makes the valence state of Cu more stable. Meanwhile, the two reduction peaks of the used catalysts both move to lower temperature, indicating that the reduction inhibiting ability of high-valent copper species decreases after the reaction.

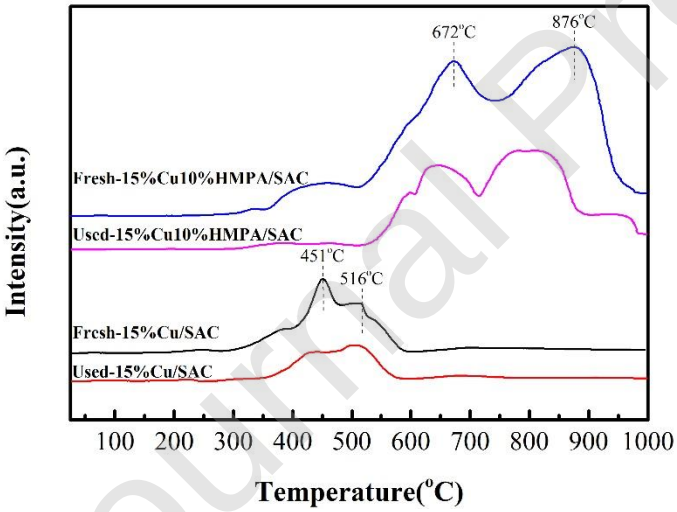

Figure 9. Temperature-programmed reduction (TPR) curves of pure Cu supported catalyst and 15%Cu10%HMPA/SAC before and after test.

XPS spectra and XAES spectra are utilized to distinguish disparate Cu species valence states on catalysts surface. The relative content of disparate states of Cu

species is calculated based on the relative deconvoluted peak area, as listed in Table S3. As shown in Figure 10a, besides the high-resolution core level spectrum of the Cu $2p_{1/2}$ and Cu $2p_{3/2}$, the two extra strong satellite peaks located at about 942.7 eV and 962.5 eV, respectively, are also discovered, illustrating that the presence of the Cu^{2+} species in catalyst [42]. From the curve fitting of Cu 2p, two main peaks with the binding energy of 934.3 eV and 954.4 eV belong to the Cu $2p_{3/2}$ and Cu $2p_{1/2}$, respectively, are ascribed to the Cu^{2+} species for Fresh-15%Cu/SAC [42-43]. Meanwhile, two other relatively small peaks located at around 932.8 eV and 953.9 eV are assigned to Cu $2p_{3/2}$ and Cu $2p_{1/2}$, respectively, confirming the existing of Cu^{+} and Cu^{0} species in catalyst, which may be generated due to the reduction by the oxidation functional group on the SAC support during the preparation process of the catalysts [44]. However, just the peaks attributed to the Cu^{2+} species can be found while the peaks ascribed to the low valence state Cu species almost disappear completely in the Fresh-15%Cu10%HMPA/SAC, indicating that the valence states Cu species in the modified catalyst are nearly all Cu^{2+}, as summarized in Table S3. As a consequence, appropriate HMPA ligand can efficiently consolidate high valence of Cu species in the synthesis process of catalyst to enhance the catalytic properties of the Cu complex catalysts. The XPS spectra of used catalysts is shown in Figure 10b. Notably, the peak at 932.8 eV corresponding to Cu^{+} and Cu^{0} is observed in the Used-15%Cu10%HMPA/SAC, illustrating that a fraction of Cu^{2+} are also reduced.

The analysis above combined with the catalytic performance of the catalysts illustrates that Cu^{2+} are the main active ingredient for the hydrochlorination of

acetylene. Hutchings and Shinoda found that the Cu^{+} species in the catalysts also possesses activity for acetylene hydrochlorination reaction [45-47]. According to the deconvolution results of the Cu LMM spectra for the used catalysts, three different peaks can be fitted including a peak located at around 918.6 eV assigned to the Cu^{0} species, a peak with a kinetic energy of 916.6 eV attributed to the Cu^{+} species and a peak at about 910.5 eV ascribed to a different Cu transition state, as shown in Figure 10c [24, 28]. Compared to the amount of Cu^{0} without any catalytic activity in pure 15%Cu/SAC (10.09%), that in the 15%Cu10%HMPA/SAC (4.52%) after the reaction decreases significantly, as listed in Table S3. Most of the reduced Cu^{2+} in the modified catalyst is changed to Cu^{+}, only a small part of Cu^{2+} is converted to Cu^{0} directly, indicating that HMPA ligand can restrain the direct reduction of the Cu^{2+} to Cu^{0} thus preventing the deactivation of the catalysts. In addition, the main elements composition on the catalysts' surface are listed in Table S4.

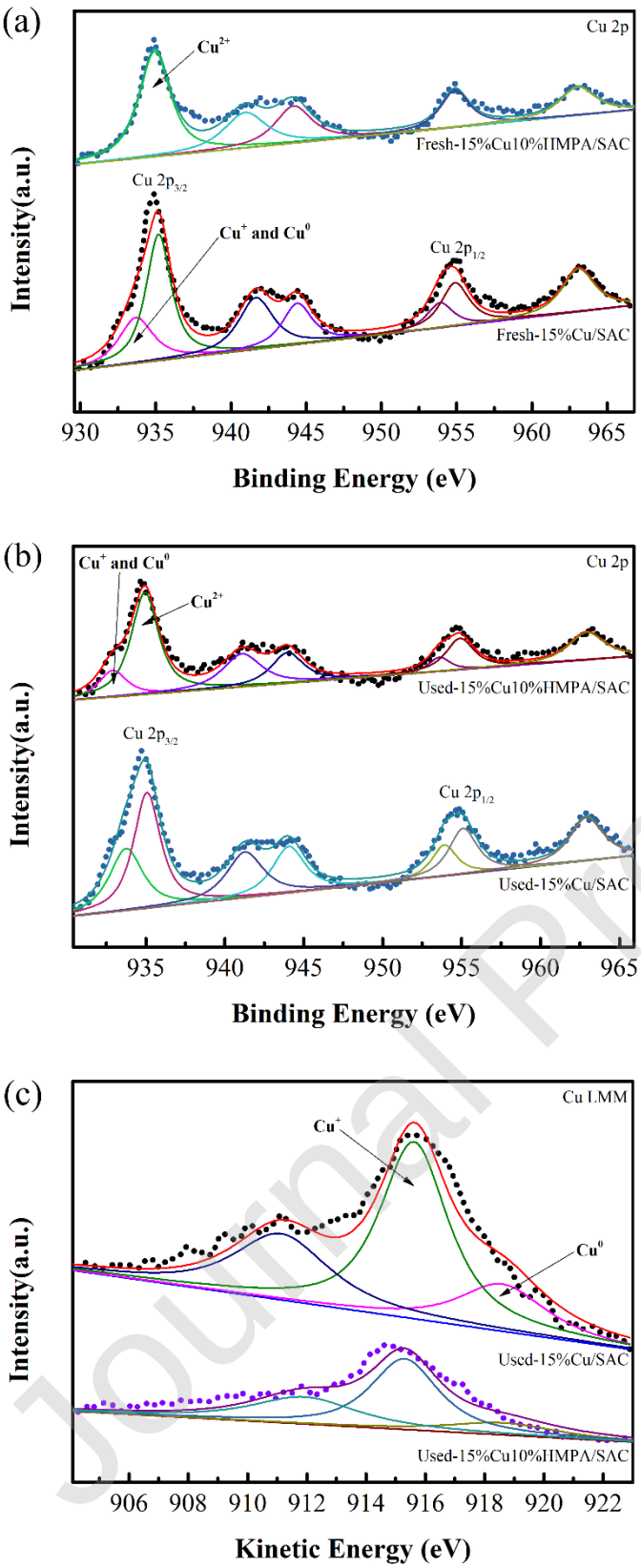

Figure 10. Cu 2p XPS spectra of fresh (a); used (b) catalysts and Cu XAES spectra of (c) used catalysts.

3.5 Coordination formation between Cu and HMPA.

The XPS spectra of O 1s can provide valid information with respect to the bond structure of the catalyst since the binding energy of O 1s electrons is an immediate consequence of the bonding between the oxygen atom and disparate cations [48]. Therefore, O 1s spectra is used to further analyze the coordination structure for Cu species and HMPA in the catalyst. As shown in Figure 11, The O 1s peak is deconvoluted into two components of fresh pure Cu supported catalyst. The peak located at 531.5 eV is attributed to non-bridging oxygen (P=O), the peak with a higher binding energy of 533.2 eV is assigned to the bridging oxygen (P-O-P) [49]. Specifically, a new deconvolution peak of the Fresh-15%Cu10%HMPA/SAC is observed at the binding energy about 532.4 eV, which is ascribed to the Cu-O-P bond since the peak position is between P=O and P-O-P [50]. Therefore, the Cu-O-P bonding is formed by bonding between the Cu in $CuCl_2$ and the O corresponding to the HMPA, indicating that the coordination bond of Cu-O is formed thus stabilizing the chemical state of Cu on catalysts surface thereby increasing the catalytic performance.

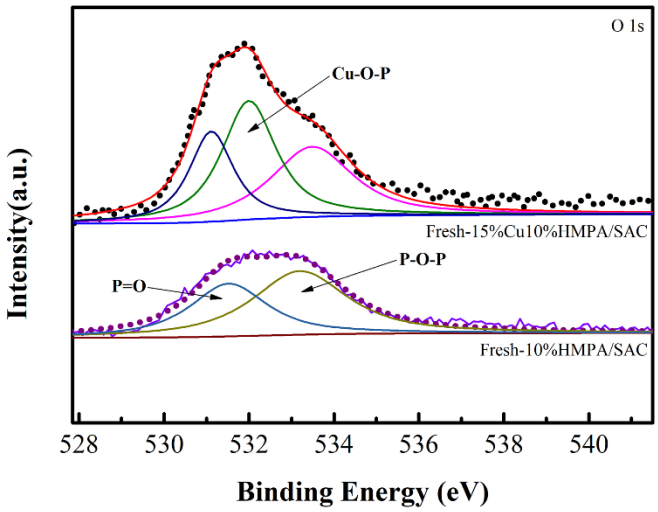

Figure 11. O 1s XPS spectra of fresh catalysts.

The FT-IR spectrums of the catalysts including 10%HMPA/SAC, pure 15%Cu/SAC, Fresh-15%Cu10%HMPA/SAC and blank control of pure HMPA are carried out to analyze the coordination structure of the catalyst based on the information for electron transfer of the characteristic functional groups, as shown in Figure 12a. Notably, the band at 1193 cm^{-1} of pure HMPA is attributed to the P=O stretching vibration [51] and the same band disappears in 10%HMPA/SAC and 15%Cu/SAC due to the strong interaction between support and HMPA but reappears at 1158 cm^{-1} in 15%Cu10%HMPA/SAC. The P=O stretching vibration of the catalyst containing both of Cu and HMPA red shifts by 35 cm^{-1} compared to that of the pure HMPA, indicating that the P=O is weakened due to the gather of electrons from C-N and CH_3- of HMPA. Meanwhile, compared to the pure HMPA, the band at 1300 cm^{-1} corresponding to the C-N stretching vibration blue shifts to 1385 cm^{-1}, which illustrates that the C-N is the electron donating group of HMPA under the electron transfer process. The band at about 2960 cm^{-1} attributed to CH_3- stretching blue shifts

to 2975 cm^{-1} of the 15%Cu10%HMPA/SAC compared with that of the 10%HMPA/SAC and 15%Cu/SAC at the same time, declaring that CH_3- strengthens due to the electron tranfer to another electron-accepting group. The results imply that the formation of the coordination structure between Cu and O in HMPA is on account of the mechanism of electron transfer among the several functional groups. In addition, the band belongs to P-O-P stretching vibration at about 751 cm^{-1} in pure HMPA red shifts drastically by 84 cm^{-1} for 15%Cu10%HMPA/SAC, which also explains that the P-O-P stretching vibration recedes due to the aggregation of electron. Subsequently, the coordinated bond of Cu-O easily establishes in 15%Cu10%HMPA/SAC because the optimal HMPA content can provide enough quantity of P-O-P [52-53].

For the purpose of further studying the coordination environment of Cu complex catalyst containing HMPA ligand, the Raman spectra for pure Cu supported catalyst and 15%Cu10%HMPA/SAC before and after reaction are measured, as shown in Figure 12b. Compared to the pure 15%Cu/SAC, a novel tiny band at 1172 cm^{-1} of Fresh-15%Cu10%HMPA/SAC is ascribed to the O-P-O symmetric stretching mode, further implying that the Cu and O constitute the coordinate bond [54]. Combined with the analysis of XPS O 1s spectra, FT-IR spectra and Raman spectra, a reasonable inference that the presence of coordination bonding between Cu and O is confirmed completely.

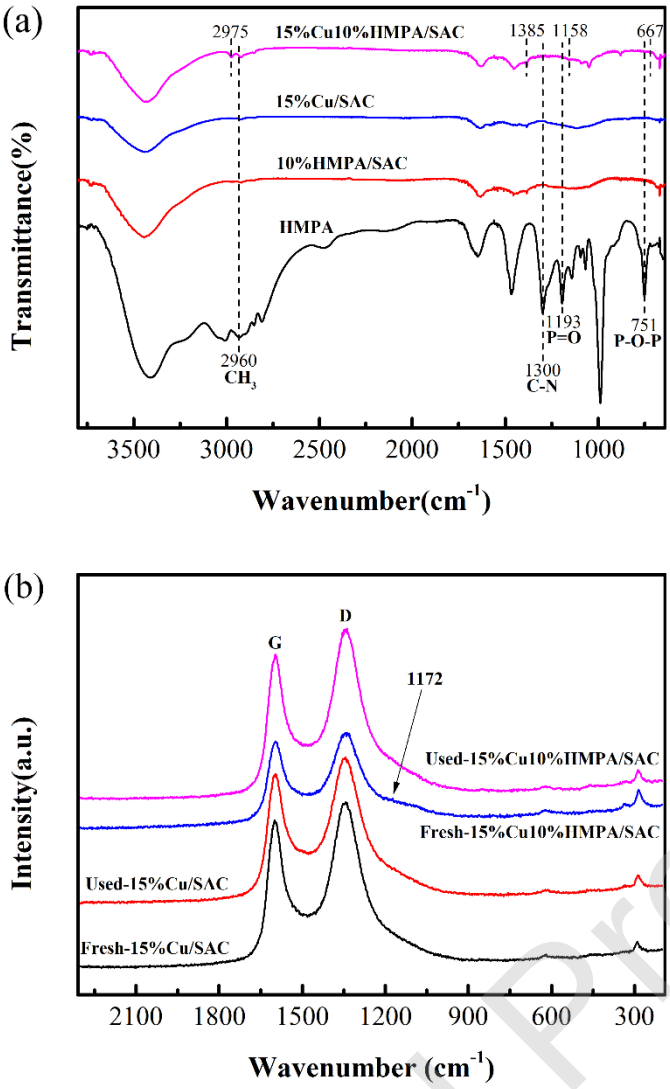

Figure 12. FT-IR spectra of (a) pure HMPA ligand and fresh carbon-supported catalysts and Raman spectra of (b) pure Cu supported catalyst and 15%Cu10%HMPA/SAC before and after test.

The DFT calculations are performed to reveal the coordination mechanism. In the stable structure of Cu complex (shown in Figure S3), the Cu interacts with the O atom in HMPA ligand, and the Cu-O distance is as short as 2.024 Å, confirming that the coordination bond between Cu and O formed. Because of the formation of Cu-O bond, the length of P=O bonds in HMPA is elongated compared to that in pure

HMPA, which is in accord with the FT-IR analysis. The Mulliken charge analysis shows HMPA loses electrons and $CuCl_2$ gets electrons when the $CuCl_2$ interacts with HMPA ligand. In particular, the H atoms of CH_3- supply electrons, while Cl atoms in $CuCl_2$ are the final electron acceptor, in which electrons are transferred through N, P, O and Cu atoms, as summarized in Table 3. The Mulliken charge of each atom is also listed in Table S5. The simulated result above revealed the formation process of coordination bonding between $CuCl_2$ and HMPA ligand from a deeper level of interatomic charge transfer, which further demonstrated the electron transfer mechanism discussed in FT-IR analysis.

Table 3. Mulliken Charges of different elements in $CuCl_2$, HMPA ligand and Cu complex.

Charge of atoms (e)	H (Total)	C (Total)	N (Total)	P	O	Cu	Cl (Total)
$CuCl_2$						0.328	-0.328
HMPA	1.785	-0.603	-1.934	1.433	-0.680		
Cu Complex	2.124	-0.773	-1.917	1.517	-0.678	0.407	-0.680

4. Conclusions

A sequence of carbon supported copper complex catalysts were synthesized with four different kinds of phosphoramide complexing agent containing P and N using the technique of incipient wetness impregnation. At the same test conditions, the catalytic activity of all modified catalysts containing phosphoamide ligands was better than that of pure 15%Cu/SAC catalysts. Notably, the 15%Cu10%HMPA/SAC catalyst exhibited the excellent catalytic performance with C_2H_2 conversion of 87.25% in the conditions of the temperature of 180 °C, the *GHSV*(C_2H_2) of 180 h^{-1} and the *V*(HCl):

$V(C_2H_2)$ of 1.2. The characterizations of XRD, TEM, TGA, ICP, H_2-TPR, XPS revealed that appropriate HMPA ligand can promote Cu loading dispersity on the SAC support, suppress catalyst surface carbon deposition, restrain the declining of Cu loading, refrain the reduction of high valence state Cu species and thus stabilizing the valent state of Cu active ingredients. Combined with the important characterizations of FT-IR, Raman spectra, O 1s XPS spectra and DFT calculations, the stable coordination bonding between Cu from $CuCl_2$ and O from HMPA ligand was testified, which was the main reason for the Cu-based catalyst with optimal HMPA contents possessed a series of outstanding qualities and owned the best catalytic activity. Furthermore, the Fresh-15%Cu10%HMPA/SAC catalyst showed a splendid stability of 100 h lifetime under the harsh condition of $GHSV(C_2H_2) = 90\ h^{-1}$ and the industrial $GHSV(C_2H_2) = 50\ h^{-1}$, indicating the catalyst modified by phosphoramide ligand especially HMPA could be a hopeful non-precious catalyst applied in hydrochlorination of acetylene.

Author Attributions Section

Hu, Yubing: Investigation, Catalyst preparation and characterization, Catalytic performance tests, Simulation work, Writing - Original draft preparation

Wang, Yan: Methodology of catalyst preparation

Wang, Yulian: Methodology of catalytic performance tests

Li, Wei: Resources

Zhang, Jinli: Resources

Han, You: Supervision, Writing- Reviewing and Editing, Project administration, Funding acquisition,

Acknowledgments

This work was supported by the National Natural Science Foundation of China (grant numbers 21978210, 21576205) and the Program for Changjiang Scholars, Innovative Research Team in University (grant number IRT_15R46).

References

[1] S.D. Pike, A. García-Trenco, E.R. White, A.H.M. Leung, J. Weiner, M.S.P. Shaffer, C.K. Williams, Catal. Sci. Technol. 7 (2017) 3842-3850.

[2] H.G. Stunnenberg, M. Vermeulen, Y. Atlasi, Science 347 (2015) 614-615.

[3] M.A. Boles, D.S. Ling, T. Hyeon, D.V. Talapin, Nat. Mater. 15 (2016) 364.

[4] T.Y. Chen, V.O. Rodionov, ACS Catal. 6 (2016) 4025-4033.

[5] S. Jones, J. Qu, K. Tedsree, X.-Q. Gong, S.C.E. Tsang, Angew. Chem. Int. Ed. 51 (2012) 11275-11278.

[6] P. Haider, A. Urakawa, E. Schmidt, A. Baiker, J. Mater. Chem. A. 305 (2009) 161-169.

[7] B.H. Wu, H.Q. Huang, J. Yang, N.F. Zheng, G. Fu, Angew. Chem. Int. Ed. 51 (2012) 3440-3443.

[8] G. Vilé, N. Almora-Barrios, S. Mitchell, N. López, J. Pérez-Ramírez, Chem. - Eur. J. 20 (2014) 5926-5937.

[9] T. Taguchi, K. Isozaki, K. Miki, Adv. Mater. 24 (2012) 6462-6467.

[10] K.B. Vu, K.V. Bukhryakov, D.H. Anjum, V.O. Rodionov, ACS Catal. 5 (2015) 2529-2533.

[11] Y. Isomura, T. Narushima, H. Kawasaki, T. Yonezawa, Y. Obora, Chem. Commun. (Cambridge, U. K.) 48 (2012) 3784-3786.

[12] M. Mastalir, E. Pittenauer, B. Stöger, G. Allmaier, K. Kirchner, Org. Lett. 19 (2017) 2178-2181.

[13] M.B. Gawande, A. Goswami, F.-X. Felpin, T. Asefa, X.X. Huang, R. Silva, X.X. Zou, R. Zboril, R.S. Varma, Chem. Rev. (Washington, DC, U. S.) 116 (2016) 3722-3811.

[14] M. del Mar Conejo, J. Cantero, A. Pastor, E. Álvarez, A. Galindo, Inorg. Chim. Acta 470 (2018) 113-118.

[15] S. Thapa, B. Shrestha, S.K. Gurung, R. Giri, Org. Biomol. Chem. 13 (2015) 4816-4827.

[16] K. Kunz, U. Scholz, D. Ganzer, Synlett (2003) 2428-2439.

[17] A.M. Kirillov, M.V. Kirillova, A.J.L. Pombeiro, Coord. Chem. Rev. 256 (2012) 2741-2759.

[18] X.X. Guo, D.W. Gu, Z.X. Wu, W.B. Zhang, Chem. Rev. (Washington, DC, U. S.) 115 (2015) 1622-1651.

[19] T.E. Schmid, S. Drissi-Amraoui, C. Crévisy, O. Baslé, M. Mauduit, Beilstein J. Org. Chem. 11 (2015) 2418-2434.

[20] E.P. Kirar, U. Grošelj, G. Mirri, F. Požgan, G. Strle, B. Štefane, V. Jovanovski, J. Svete, J. Org. Chem. 81 (2016) 5988-5997.

[21] T. Liu, H. Fu, Synlett 44 (2012) 2805-2824.

[22] S. Layek, B. Agrahari, S. Dey, R. Ganguly, D.D. Pathak, J. Organomet. Chem. 896 (2019) 194-206.

[23] S.-N. Zhao, X.-Z. Song, S.-Y. Song, H.-j. Zhang, Coord. Chem. Rev. 337 (2017) 80-96.

[24] X.M. Wang, M.Y. Zhu, B. Dai, ACS Sustainable Chem. Eng. 7 (2019) 6170-6177.

[25] J.L. Zhang, N. Liu, W. Li, B. Dai, Front. Chem. Sci. Eng. 5 (2011) 514-520.

[26] J.H. Xu, J. Zhao, J.T. Xu, T.T. Zhang, X.N. Li, X.X. Ding, J. Ni, J.G. Wang, J. Cen, Ind. Eng. Chem. Res. 53 (2014) 14272-24281.

[27] Y.F. Ren, B.T. Wu, F.M. Wang, H. Li, G.J. Lv, M.S. Sun, X.B. Zhang, Catal. Sci. Technol. 9 (2019) 2868-2878.

[28] H. Li, F.M. Wang, W.F. Cai, J.L. Zhang, X.B. Zhang, Catal. Sci. Technol. 5 (2015) 5174-5184.

[29] Y.Y. Zhai, J. Zhao, X.X. Di, S.X. Di, B.L. Wang, Y.X. Yue, G.F. Sheng, H.X. Lai, L.L. Guo, H. Wang, X.N. Li, Catal. Sci. Technol. 8 (2018) 2901-2908.

[30] K. Zhou, J.K. Si, J.C. Jia, J.Q. Huang, J. Zhou, G.H. Luo, F. Wei, RSC Adv. 4 (2014) 7766-7769.

[31] Y. Wang, Y Nian, J.L. Zhang, W. Li, Y. Han, Mol. Catal. 479 (2019) 110612.

[32] L. Li, Z.H. Zhu, Z.F. Yan, G.Q. Lu, L. Rintoul, Appl. Catal., A 320 (2007) 166-172.

[33] S.S. Shang, W. Zhao, Y. Wang, X.Y. Li, J.L. Zhang, Y. Han, W. Li, ACS Catal. 7

(2017) 3510-3520.

[34] W. Zhao, W. Li, J.L. Zhang, Catal. Sci. Technol. 6 (2016) 1402-1409.

[35] J. Wang, T.F. Zhang, Z.X. Song, P. Ning, K.X. Long, B. Zhao, J.H. Huang, Q.L. Zhang, Res Chem Intermed 44 (2018) 2333-2346.

[36] S.M. Sajjadi, M. Haghighi, Int J Energy Res. 43 (2019) 853-873.

[37] A. Serrano-Lotina, L. Daza, Appl. Catal., A 474 (2014) 107-113.

[38] W.J. Lee, C.Z. Li, Carbon 46 (2008) 1208-1217.

[39] Y.Z. Dong, W. Li, Z. Yan, J.L. Zhang, Catal. Sci. Technol. 6 (2016) 7946-7955.

[40] Y.Z. Dong, H.Y. Zhang, W. Li, M.X. Sun, C.L. Guo, J.L. Zhang, J. Ind. Eng. Chem. (Amsterdam, Neth.) 35 (2016) 177-184.

[41] F.-W. Chang, H.-C. Yang, L.S. Roselin, W.-Y. Kuo, Appl. Catal., A 304 (2006) 30-39.

[42] H.P. Li, R.Q. Cheng, Z.L. Liu, C.F. Du, Sci. Total Environ. 683 (2019) 638-647.

[43] M. Faheem, X.B. Jiang, L.J. Wang, J.Y. Shen, RSC Adv. 8 (2018) 5740-5748.

[44] K.L. Deutsch, B.H. Shanks, J. Catal. 285 (2012) 235-241.

[45] G.J. Hutchings, J. Catal. 96 (1985) 292-295.

[46] M. Conte, A.F. Carley, G. Attard, A.A. Herzing, C.J. Kiely, G.J. Hutchings, J. Catal. 257 (2008) 190-198.

[47] D. von Deak, E.J. Biddinger, K.A. Luthman, U.S. Ozkan, Carbon 48 (2010) 3635-3658.

[48] G.D. Khattak, A. Mekki, M.A. Gondal, Appl. Surf. Sci. 256 (2010) 3630-3635.

[49] D. Raskar, M.T. Rinke, H. Eckert, J. Phys. Chem. C 112 (2008) 12530-12539.

[50] M.A. Salim, G.D. Khattak, M.S. Hussain, J. Non-Cryst. Solids 185 (1995) 101-108.

[51] A.M. Puziy, O.I. Poddubnaya, A. Martínez-Alonso, F. Suárez-García, J.M.D. Tascón, Carbon 40 (2002) 1493-1505.

[52] A. Chahine, M. Et-tabirou, Phase Transitions 75 (2002) 309-314.

[53] S.S. Sastry, B.R.V. Rao, Phys. B (Amsterdam, Neth.) 434 (2014) 159-164.

[54] A. Chahine, M. Et-tabirou, M. Elbenaissi, M. Haddad, J.L. Pascal, Mater. Chem. Phys. 84 (2004) 341-347.